Article

The Effects of Dominant Driving Forces on Summer Precipitation during Different Periods in Beijing

Fuxing Li [1,2] and Li He [1,*]

[1] Key Laboratory of Water Cycle and Related Land Surface Processes, Institute of Geographic Sciences and Natural Resources Research, Chinese Academy of Sciences, Beijing 100101, China; lifuxing6042@163.com
[2] University of Chinese Academy of Sciences, Beijing 100101, China
[*] Correspondence: heli@igsnrr.ac.cn; Tel.: +86-10-6488-8151

Abstract: Wavelet analysis methods (CWT, XWT, WTC) were employed to evaluate the impact of dominant climatic driving factors on summer precipitation in the Beijing area based on monthly precipitation data of Beijing ranging from 1880 to 2014. The two climatic driving factors, i.e., the East Asian summer monsoon (EASM) and the Northern Limit of Western Pacific Subtropical High (NWPSH) were considered in particular. The relationships between summer precipitation and EASM/NWPSH were also examined. The results revealed similar periods in low-frequency oscillation (76–95 years) and mid-range frequency oscillation (32–60 years) for the summer precipitation in the Beijing area and EASM/NWPSH. The summer precipitation correlated positively with the NWPSH and EASM, especially for periods of 43 years and 33 years, respectively. This indicates that summer precipitation during 1880–1960 and during the years after 1960 was significantly affected by NWPSH and EASM, respectively. Based on the periodic change of 33 years for both summer precipitation and EASM, heavy precipitation can be expected to occur again in Beijing at approximately 2026. Understanding the relationships between summer precipitation and climatic factors is of significant importance for precipitation predictions and water resource variations in the Beijing area.

Keywords: precipitation; EASM; NWPSH; wavelet analysis; Beijing

1. Introduction

The impact of climatic factors on the regional hydrological process has been paid close attention to by meteorologists and hydrologists [1–5]. As a major aspect of the water circulation system, spatial-temporal distribution of regional precipitation is inevitably affected by climatic factors; thus further inducing a series of hydrologic disasters, including drought and flood [6–8]. Therefore, the investigation of climatic factors affecting regional precipitation is of vital significance for the prevention of natural disasters and for regional water resources allocation.

Considerable research has been written outlining the influence of climatic factors on the regional precipitation [1,9–12]. For instance, the monsoon circulations were often considered as the primary driver in the variability of regional summer precipitation over the world [13–17]. The North American monsoon (NAM) contributes to one-half of the annual precipitation in the southwestern United States [18]. Moreover, Lahmers et al. [19] found that the presence of transient inverted troughs is associated with extreme precipitation over the southwestern contiguous United States during the early monsoon season. Djebou [20] investigated the precipitation alterations over the Niger River basin in West Africa. He found that the precipitation in the basin is primarily controlled by the West African monsoon circulation, for which the local vapor accounts for 27% of the annual precipitation. Previous studies indicated that the monsoon circulations play a role in the regional summer precipitation.

Typical continental monsoon climate prevails in Beijing as the political, economic, and cultural center of China, which is located in the North China [21–24]. The East Asian summer monsoon (EASM) strongly affects the precipitation of this area. The stronger summer monsoon can easily carry large amounts of vapor into the northern inland of China (including North China), which in turn increases the precipitation, and vice versa [25–28]. As an important aspect of atmospheric circulation, the Western Pacific Subtropical High (WPSH) is one of the permanent large-scale circulation systems, controlling the weather and climate of tropical and subtropical regions. Downdraft prevails in the subtropical high control area with low precipitation, high temperature, and drought, while intense convection leads to more precipitation in the marginal area. Therefore, the activity of WPSH is closely related to the climate of China [29]. The vapor current is effortlessly transported into North China when the ridge line and northern limit position of subtropical high are more north and maintain an anticyclonic flow. As an important aspect of this particular climate system, EASM has perceptibly changed during the past few decades, resulting in a significant variation of summer precipitation in the Beijing area. However, the precipitation variation demonstrates some deviation due to the differences in advance and retreat time, strength, and influence scope of WPSH. Recently, a significant research effort has been devoted to the spatial-temporal variation of precipitation in the Beijing area and its response to the EASM and the WPSH [30–34]. The inter-annual and inter-decadal variations of precipitation in the Beijing area are apparent. The precipitation amount during the 21st century decreased by 100 mm compared to those during the 1990s [35]. Li et al. [36,37] investigated the periodic variation of precipitation in the Beijing area at multi-timescales employing wavelet analysis. The acquired results indicated that the time series of precipitation with 286 years for the Beijing area demonstrated significant periodic variations in 85 years, 35 years, and 21 years. Additionally, the precipitation in spring, summer, autumn, and winter corresponded to a strong periodic variation of 30–170 years, 80–95 years, 75–95 years, and 55–66 years, respectively. The EASM was considered to be the key climatic factor, affecting the inter-decadal variation of summer precipitation of the Beijing area [28]. Zhu et al. [38] studied the inter-decadal oscillation of summer precipitation in the Beijing area and its correlation with EASM and the results indicated that the summer precipitation of the Beijing area correlated positively with the EASM index (EASMI), especially in the 80-year oscillation period. However, a further study performed by Gao et al. [39] denoted that the relationship between summer precipitation of North China and the subtropical high transformed from a weak negative correlation to a strong positive correlation since the 1990s, caused a change in relationship from positive correlation to negative correlation between summer precipitation and EASM. These previous studies demonstrate that precipitation in the Beijing area changed significantly during inter-annual and inter-decadal time scales, which is affected by the EASM and WPSH.

However, the majority of these studies focused on periodic variations of precipitation in Beijing or North China, while the impact of dominant climatic driving factors on the precipitation at multi-timescales was less investigated [40]. Moreover, it should be noted that the investigation and distinguishing of dominant driving factors on summer precipitation during different periods would be of great significance for a correction of periodic variation of precipitation and for the prediction of future water resources. Therefore, based on the integrated summer precipitation data (June to September) during 135 years (1880–2014) of the Beijing area, the present study analyzed periodic variations of the summer precipitation and EASM/NWPSH (the Northern Limit of Western Pacific Subtropical High) using continuous wavelet transformation (CWT). Subsequently, the cross wavelet transform (XWT) was employed to investigate prospective correlations between precipitation and EASM/NWPSH, the intimacy of which was further quantified by wavelet coherence analysis (WTC). Finally, the intimacy was utilized to analyze the periodic driving rules of dominant driving factors on precipitation during different periods.

2. Study Area

Beijing city is situated downstream of the Haihe Basin and is surrounded by the Hebei province and Tianjin city, with a total area of 16,800 km². Mountainous land and plain compose the main structure of the area, which crosses the second and third steps with an altitude drop of 2200 m (Figure 1). The Taihang-Yan Mountain and the North China Plain range from the northwest to the southeast, and account for 62% and 38% of total area, respectively.

Beijing is located in semi-humid and semi-arid regions, and is a typical representative for continental monsoon climate. Northerly wind prevails during winter with low temperatures and precipitation under the control of cool-dry high pressure from Mongolia. Southeasterly wind prevails in summer with high temperature and precipitation under the control of Pacific warm-humid high pressure. Multi-year average precipitation and temperature values are 600 mm and 12 °C, respectively, and the precipitation during summer (June to September) accounts for 81% of the annual total.
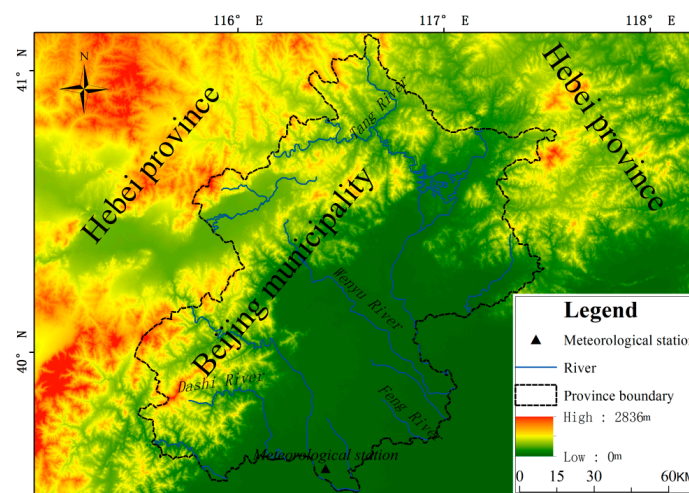

Figure 1. Topographic map of the Beijing area.

3. Data and Method

3.1. Data Source

Analyzed data in the present study includes: (a) the precipitation time series of the Beijing area from 1880 to 2014; (b) the East Asian Summer Monsoon index (EASMI) from 1880 to 2014; and (c) the NWPSH index from 1880 to 1999. In this study, we standardized the time series (zero mean, unit standard deviation) and will refer to the standardized versions simply as precipitation, EASMI, and NWPSH. The Beijing meteorological station is located at $39°48'$ latitude and $116°28'$ longitude.

3.1.1. Precipitation Data

The precipitation data from 1880 to 2014, which was observed with modern instrumentation, was acquired from the Beijing Meteorological Station. Currently, many studies [35–37] have been devoted to the data to analyze the variation of the precipitation in the Beijing area. Given that the impact of EASM on the precipitation lags one month, the present study employed the sum amount of precipitation during June to September as the summer precipitation.

3.1.2. Index of EASM

This study adopts the EASMI defined by Guo [41]. Many indices have been proposed to quantify the EASM [42–44]. Among these indices, the EASMI defined by Guo [41] is based on the formative mechanism of the EASM and calculated as the difference of the monthly average air pressure during

the summer season (June, July, and August) at sea level between the Asian Continent (110° E) and the Pacific Ocean (160° E) in the range of 10°–50° N. The procedures of EASMI calculation can be accessed via Guo [41]. The EASMI during 1880–2000 was quoted from the data, which Guo presented in reference [45]. The 6 h sea-level pressure (SLP) data of the Northern Hemisphere during the period of 2001–2014 provided by National Centers for Environmental Prediction (NCEP) and National Center for Atmospheric Research (NCAR) (available online: http://rda.ucar.edu/datasets/ds090.0/, with a horizontal resolution of 0.25°), as well as the calculation method, which Guo [41] referred to in reference were employed to arrive at an average EASMI of July to August during 2001–2014.

3.1.3. Northern Limit of West Pacific Subtropical High

NWPSH during 120 years (1880–1999) that was utilized in the present study was derived from the indicator calculated by Mu [46], as shown in reference [46].

3.2. Method

Despite being a newly developed mathematical method, the wavelet method has significant advantages compared to other analytical methods in terms of multi-resolution, localization, and multi-level factors [47,48]. Recently, many studies [49–51] have been devoted to this method for hydro-meteorological research, producing a string of scientific achievements, especially in multiple-scale climate diagnosis studies [52–56].

3.2.1. Continuous Wavelet Transform (CWT)

The CWT analysis employs wavelet functions to expand the time series into the time-frequency space to ultimately find its localized intermittent periodicities [57]. The wavelet functions are a class of functions with zero means localized in both frequency and time. Different types of wavelet functions can be utilized in the CWT analysis. Among these, the Morlet wavelet function can provide reasonable localization in both time and frequency space, and was therefore adopted in the present study. The Morlet wavelet function can be expressed as [53]:

$$\psi_0(\eta) = \pi^{-1/4} e^{iw_0\eta} e^{-1/2\eta^2} \tag{1}$$

where $\psi_0(\eta)$ denotes the wavelet function; η = dimensionless time; and w_0 = dimensionless frequency. In the present study, $w_0 = 6$ was adopted. Given a discrete time series of observation $s = \{s_1, s_2, \dots, s_n\}$, the CWT analysis of s can be expressed as:

$$W_n^x(s) = \sum_{n'=0}^{N-1} x_n \psi^* \left[\frac{(n'-n)\delta t}{s} \right] \tag{2}$$

where $W_n^x(s)$ denotes the wavelet coefficient, n = localized time index; N = the number of observations; s = wavelet scale; δt = sampling period; N = number of points in the time series, and the asterisk (*) indicates the complex conjugate. $|W_n^x(s)|^2$ is defined as the wavelet power.

3.2.2. Cross Wavelet Transform (XWT)

XWT is a new statistical signal approach that combines with the CWT and the cross spectra analysis, which is utilized to investigate the correlation of two time series in multi-timescales from the time-frequency domain [53].

The XWT of two time series X and Y is defined as $W_n^{XY}(s) = W_n^X(s) W_n^{Y*}(s)$. The cross wavelet power is defined as $|W_n^{XY}(s)|$ and indicates the common high power area. The higher the value of $|W_n^{XY}(s)|$ in the areas, the more significant the correlation of two time series will be.

The theoretical distribution of the cross wavelet power of two time series with background power spectra P_k^X and P_k^Y is given in Torrence and Compo [58] as:

$$\frac{\left|W_n^X(s)W_n^{Y*}(s)\right|}{\sigma_X \sigma_Y} = \frac{Z_v(P)}{v}\sqrt{P_k^X P_k^Y} \tag{3}$$

where σ_X, σ_Y denote the standard deviation of two time series X and Y, respectively. $Z_v(p)$ is the confidence level associated with the probability p for a probability density function (pdf) defined via the square root of the product of two χ^2 distributions. The 5% significance level is calculated using $Z_2(95\%) = 3.999$ [53].

The complex XWT angle indicates the local relative phase relationship of two time series in the time-frequency domain. In the XWT method, the circular mean of the phase over regions with higher than 5% statistical significance, which is outside the cone of influence (COI), was used to quantify the phase relationship. The circular mean is defined as:

$$\alpha = \arg(X, Y); X = \sum_{i=1}^{n}\cos(\alpha_i); Y = \sum_{i=1}^{n}\sin(\alpha_i) \tag{4}$$

In the Cross Wavelet Spectrum, the relative phase relationship of two time series is displayed with arrows. The arrows point down and up, when the *Y*–time series lead 1/4 and 3/4 periods ahead of time series *X*, respectively. However, the arrows point left (anti-phase) and right (in-phase), when the *Y*–time series lead the *X*–time series by 1/2 and 1 period, respectively.

3.2.3. Wavelet Coherency (WTC)

The WTC is used to evaluate the level of coherence of the cross wavelet transform in the time frequency space. The two time series can also indicate a significant correlation in the WTC spectrum, even though it exits in low common power areas for two time series in the XWT spectrum [56]. The WTC is defined as:

$$R_n^2(s) = \frac{\left|S\left(s^{-1}W_n^{XY}(s)\right)\right|^2}{S\left(s^{-1}\left|W_n^X(s)\right|^2 \times s^{-1}\left|W_n^Y(s)\right|^2\right)} \tag{5}$$

where *S* is a smoothing operator in the time frequency space. A Monte Carlo approach was utilized with a red noise to compute the statistical significance of the correlation [59].

4. Results and Discussion

4.1. Variation of Summer Precipitation and EASMI/NWPSH at Multi-Timescales

Figure 2 illustrates the continuous wavelet transformation spectrum and whole wavelet spectrum of Beijing precipitation, EASMI, and NWPSH. The periodic signals in the time-frequency domain show distinct differences for the precipitation and EASMI/NWPSH at different time scales, while a main period oscillation exists within the time series. The CWT analysis may suffer from edge effects because of an incomplete localization in time. Therefore, the COI was depicted in Figure 2 to indicate the region where edge effects can be neglected.

The wavelet spectrum of EASMI shows a considerable amount of high power in the approximately 80-year band spread through the study periods, and the center of oscillation occurred around the 1970s. A less significant power resided over the 40 to 50 year band from 1880 to 1960, with an oscillation center at 1910, while the oscillation gradually weakened after 1960 (Figure 2a). Guo [45] also found that the EASM oscillates with two long-term periods of approximately 40 years and 80 years, which is consistent with the results of the present study. Although a 128-year band showed significant high power during the whole study period, it cannot be assessed due to the limited length of the data record

(142 years). In addition, decadal oscillations at 16 years and 25 years are seen during the periods of 1950–1980 and 1880–1990, respectively.

The wavelet spectrum of NWPSH is shown in Figure 2b. The most pronounced variability within the wavelet power spectrum for the NWPSH was observed during the periodicity band of 40 years through the study periods, with an oscillation center at around 1920, which is basically consistent with the result reported by Mu [46]. The longer decadal variations (~96 years) cannot be assessed with statistical significance given the comparatively short length of the study record (120 years). In addition, the inter-annual oscillations at 4–8 years and decadal oscillations at ~20 years have been seen in the periods of 1890–1910 and 1950–1999.

Figure 2c shows the wavelet spectrum of summer precipitation in Beijing from 1880 to 2014. The most pronounced variability within the wavelet power spectrum was observed during the periodicity band of 80–95 years from 1880 to 2014 associated with oceanic-atmospheric patterns (e.g., EASM or NWPSH). A 32–60 year period dominates the years from 1880 to the current day with significant oscillation. Ding et al. [28] also found that the precipitation in North China oscillates in the dominant period of 80 years and the minor period of 30–40 years, and the weakening EASM during the past 54 years results in a distinct decrease of water vapor source for the precipitation over North China. Zhu et al. [38] reported a distinct 80-year oscillation of summer precipitation in North China based on magnitude data of the last 530 years of precipitation in Eastern China, which corresponded well with EASM at periodic component of 80 years. The inter-annual oscillations at 2–4 years as well as 4–8 years can be seen in the periods of 1880–1900, 1910–1930, and 1940–1980, all of which were significant at a 95% confidence level. Decadal oscillations at ~20 years can be seen in the period of 1880–1910, and are significant at a 95% confidence level.

Although the wavelet power of the precipitation in the Beijing area and the EASMI/NWPSH show similar periodic oscillations at multi-timescales, it is hard to identify a pattern of correlation by sight between the EASMI/NWPSH and precipitation in the Beijing area in the CWT. Therefore, XWT was employed to further investigate phase correlations between Beijing precipitation and EASMI/NWPSH.
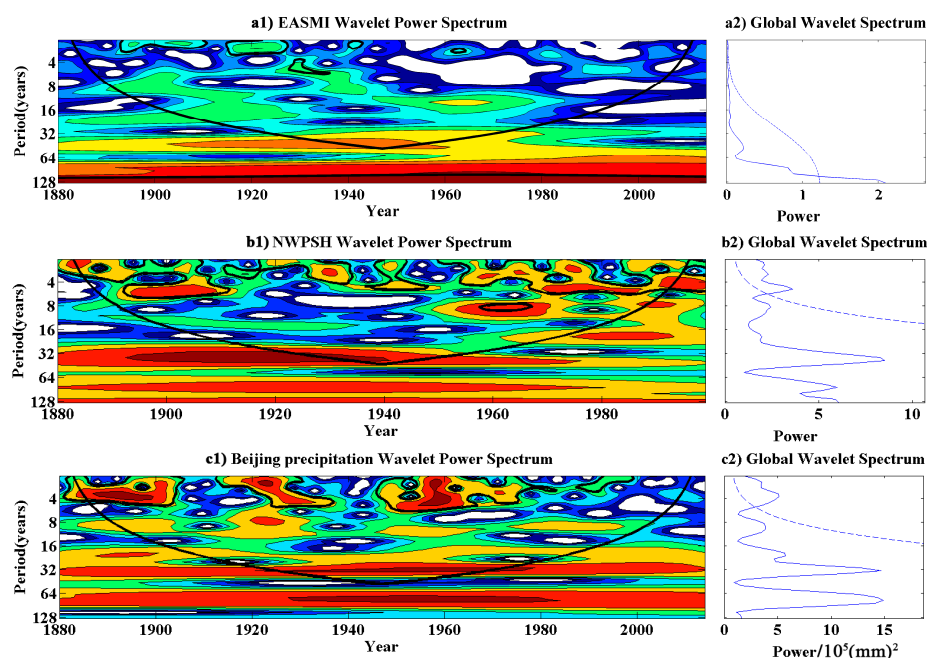
Figure 2. Continuous wavelet transform ((**left**), red color means stronger power and blue means weakest power) and global wavelet spectrum (**right**) of East Asian Summer Monsoon index (EASMI) (**a**); Northern Limit of Western Pacific Subtropical High (NWPSH) (**b**); precipitation of the Beijing area (**c**).

### 4.2. Time-Frequency Analysis of Precipitation and EASMI/NWPSH

The XWT was performed in order to identify the relationships between precipitation and the EASMI/NWPSH (Figure 3). The common power features indicate a similar periodic variation between two signals, and the directions of arrows in the time-frequency domain denote phase relations of both signals.

Figure 3 shows the cross wavelet spectrum for the Beijing precipitation and EASMI/NWPSH. The red region represents the common high-energy region of two signals at different timescales. More red denotes stronger similarities, while the blue regions represent low-energy areas, indicating weak similarity. The XWT for precipitation in the Beijing area and the EASMI (Figure 3a) share a common power area in the inter-annual oscillations of 2–4 years from 1880 to 1900, 1910 to 1930, and 1960 to 1970. Arrows that point right in the common areas indicate that the areas within a 2–4 year period are positively in-phase (phase-locked), and that the results are significant at the 95% confidence level.

Many studies [60,61] further indicated that the precipitation over North China oscillates at quasi 2–3 years. For instance, Hartmann et al. [62] employed the wavelet analysis as well as the auto-correlation and spectrum analysis (ASA) to investigate precipitation variations of China based on the data from 132 meteorological stations, indicating that the quasi 2–3 years oscillations of precipitation prevailed over China. In addition, the ~32 year period areas reveal some common cross wavelet power from 1920 to 2014 (although not with 95% significance). Furthermore, the areas within a ~32 year period are positively in-phase (phase-locked). This demonstrates that large multiple years present decadal variations in the precipitation that closely relate to a strong EASMI signal. When a stronger EASM year happens, the precipitation in the Beijing area has possibly a larger increase. In other words, the EASM is an important factor in the precipitation forecasting for the Beijing area.

The cross power spectrum between precipitation in the Beijing area and NWPSH (Figure 3b) shows a significant common power at 2–4 years with an ambiguous phase relation in the periods of 1890–1900, 1920–1930, and 1960–1965, which are all significant at a 95% confidence level. There was a rather large area of high common power at 28–50 year scales from 1880 to 1960. The common power at 28–50 year scales shows an apparent in-phase relation, and the result is significant at a 95% confidence level during 1880–1960. This suggests that the precipitation in the Beijing area is closely related to the NWPSH at 28–50 year scales. The in-phase relation furthermore indicates that the NWPSH is an important factor in the precipitation over the Beijing area. Similar results were also obtained in other studies [46].

The results shown in Figure 3 confirm that the common XWT power between precipitation in Beijing and the EASMI/NWPSH were indeed high, indicating a close relationship between precipitation and the EASMI/NWPSH. To quantify the intimacy of the correlation between precipitation and the EASMI/NWPSH, the WTC was employed.
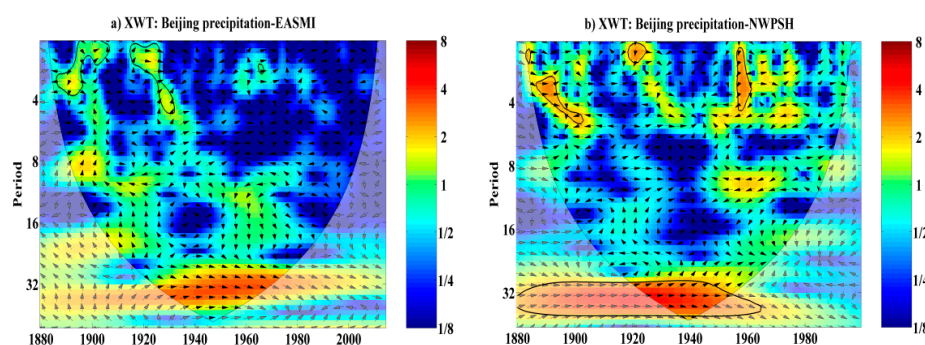
Figure 3. Cross Wavelet Spectrum between EASMI (**a**) and NWPSH (**b**) and the precipitation of the Beijing area.

4.3. Intimacy Analysis of the Correlation between Precipitation and EASMI/NWPSH

CWT and XWT were employed to investigate the common properties between two time series; however, these cannot quantify the correlation between two variables. Therefore, the WTC was employed to quantify the intimacy of the correlation between precipitation in the Beijing area and the EASMI/NWPSH.

The wavelet coherence results between precipitation and the EASMI/NWPSH are shown in Figure 4. The WTC between the EASMI and the precipitation in the Beijing area shows common significant regions during 1960–2014 in the 28–35 year period valued as high as 0.8, and the results were significant at the 95% confidence level. The arrows pointing right in the common regions during the 28–35 year period indicate a significantly positive relation. This suggests that a pattern based on the 28–35 year period of the EASM could have predictive skills for the precipitation of the Beijing area; i.e., the precipitation may reflect EASM-like variability during this period. In the high frequency oscillation, the precipitation is also closely related to the EASM at an average of 0.8 in the inter-annual oscillations of 2–4 years and ~8 years with unclear phase relation.

The WTC results between NWPSH and the precipitation in the Beijing area are shown in Figure 4b. A high coherence is apparent at 2–4 year timescales with ambiguous phase relation during 1880–1890, 1950–1960, and 1970–1980, and the coherence is significant at a 95% confidence level. The WTC of precipitation in the Beijing area and the NWPSH show much less significant correlations with small areas sparsely distributed around 4–8 years and 10–16 years periods. Some of these areas reveal a high correlation; however, too small for a 95% significance level. However, the WTC between precipitation and the NWPSH shows significant areas in the 32–50 year periods valued at 0.8 throughout the entire study period, and the coherence was significant from 1880 and 1960. This suggests a strong correlation between NWPSH and the precipitation in the Beijing area, indicating that NWPSH could be a predictive climatic factor for the precipitation during 32–50 year periods.

Based on these results, the EASMI/NWPSH has an important impact on the precipitation in the Beijing area at inter-annual time scales (2–4 years) and inter-decadal time (~33 and ~43 years). Furthermore, the precipitation in the Beijing area significantly correlated with the EASMI/NWPSH in the ~33 and ~43 year periods, with a value of 0.8. This correlation reflects a combination of the strong precipitation EASM/NWPSH signal, indicating that the EASM and NWPSH are important climatic drivers for the precipitation in the Beijing area for the multi-decadal scale (e.g., ~33 years for EASM and ~43 years for NWPSH).
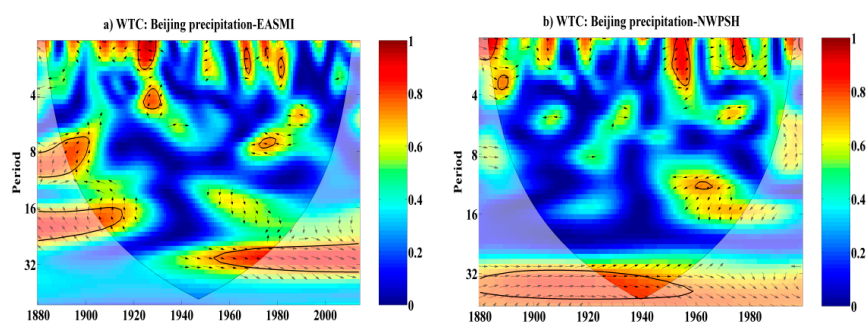
Figure 4. Wavelet Coherence Spectrum between EASMI (**a**); NWPSH (**b**) and precipitation of the Beijing area.

4.4. Relationship between EAMSI/NWPSH and the Precipitation at Inter-Decadal Time Scale

In an attempt to display the significant correlation between the precipitation in the Beijing area and the EASMI/NWPSH, four cutting lines parallel to *x*-axis on the values mentioned above (~33 years for EASMI/precipitation, ~43 years for NWPSH/precipitation) respectively were made in Figure 2, and then the intersection points on each cutting line with Figure 2 formed a time series

of Morlet wavelet coefficients in the period of 1880–2014 for EASMI/precipitation and 1880–1999 for NWPSH/precipitation, as shown in Figure 5a. The time series of Morlet wavelet coefficients are defined as the oscillation components of precipitation and EASMI/NWPSH at ~33 year and ~43 year timescales. In addition, the time series of precipitation and EASMI/NWPSH are also shown in Figure 5c,d.

The ~33 year oscillation component of the precipitation in the Beijing area corresponds positively to the ~33 year component of EASM (Figure 5a) from 1930 to 2014. This revealed that the summer precipitation in the Beijing area was above normal when the EASMI was higher, and vice versa. Based on the periodic variation of precipitation and an EASMI at a ~33 year time scale, heavy precipitation in the Beijing area will likely occur again in approximately 2026. This suggests that the EASM could be a forecasted climatic factor for the precipitation in the Beijing area in a ~33 year period, especially subsequent to the 1960s. In addition, the precipitation in the Beijing area shows synchronous variations as well as the EASMI (Figure 5c), with decreasing periods of 1880–1900, 1920–1940, and 1960–2000 and increasing periods of 1900–1920, 1940–1960, and 2000–2014. In contrast, the ~43 year oscillation component of the precipitation in the Beijing area corresponds positively with that of the NWPSH (Figure 5b) from 1880 to 1960. This revealed that the precipitation in the Beijing area is closely related to the NWPSH at a ~43 year time scale. The positive relation indicates that an NWPSH closer to north would cause a larger amount of summer precipitation in the Beijing area. However, the correlation between precipitation and NWPSH gradually weakened after 1960, and the signal of precipitation during this period oscillates weakly. The impacts of EASM on precipitation possibly weaken the correlation between precipitation and the NWPSH. Similar to the pattern of the ~43 year oscillation, the NWPSH and the precipitation changed synchronously from 1880 to 1960, with decreasing periods of 1880–1900 and 1920–1940 and increasing periods of 1900–1920 and 1940–1960. Furthermore, the variations of precipitation and the NWPSH were not synchronized after 1960 (Figure 5d).
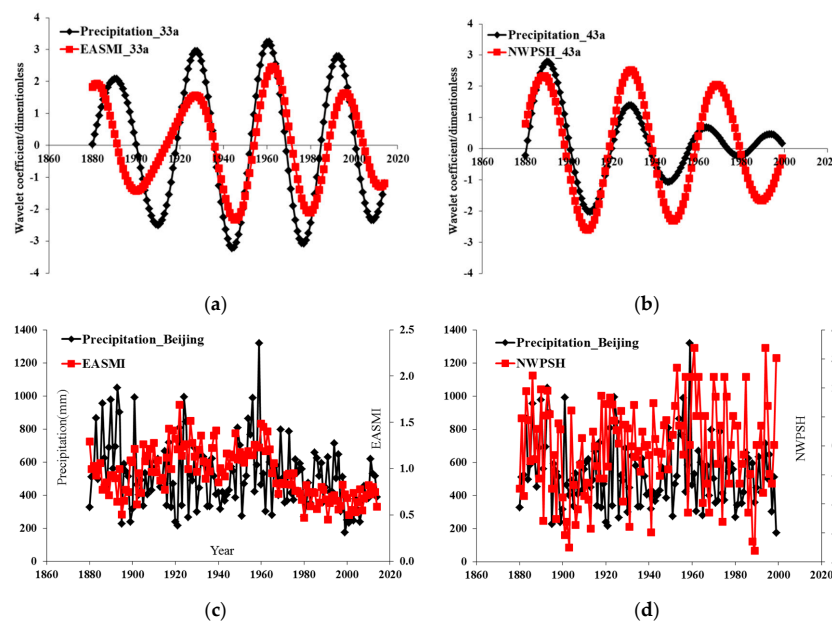
Figure 5. Related periodic components and variations of Beijing summer precipitation and the EASMI (**a**,**c**)/NPWSH (**b**,**d**).

In addition to EASM and WPSH, the pacific decadal oscillation (PDO) and El Niño-Southern Oscillation (ENSO) also affect the climate of China. These were considered to be closely related to the summer precipitation of the Yangtze River basin and the Huaihe River basin of China [63,64]. Moreover, ENSO also related to the anomaly of inter-annual precipitation of North China [65]. As a

major aspect of the global climatic system, PDO also significantly influences the climate change of the Pacific Rim. A previous study [66] reported that the negative phase pattern of PDO has transformed into a positive phase pattern since the mid-1970s. The phase transition of PDO weakened the intensity of EASM by affecting the circulation system of EASM, which in turn resulted in less precipitation in North China. Nevertheless, given the direct and dominating impact of the circulation systems of EASM and WPSH on the climate of East China, only these two main climatic driving factors were analyzed in the present study. The results indicate that the precipitation in Beijing was linked to the variation of EASMI/NWPSH at both high and low frequency time scales. The positive relationship between precipitation in the Beijing area and EAMSI/NWPSH was significant at time scales of ~33 years and ~43 years, respectively (i.e., stronger EASM and WPSH closer to the North could introduce larger amounts of precipitation to the Beijing area). However, the correlation between NWPSH and summer precipitation of Beijing gradually weakened subsequent to 1960, while EASM still exerted a strong impact on precipitation. This could be the forecasted climatic factor for the prediction of precipitation and water resources in the Beijing area.

However, non-climatic elements also have impacts on the summer precipitation over Beijing area in spatial terms. The expanded urban land cover and increased aerosols of the Greater Beijing Metropolitan Area restrained the precipitation processes, leading to suppressed convection and rainfall over the northwest area, and enhanced convection and more precipitation in the southeast region [67,68]. Influenced by the topography, annual precipitation of the plain area of Beijing area is more than that of the mountainous area [35].

5. Conclusions

The present study investigated the correlation between precipitation in the Beijing area and EASM/NWPSH using comprehensive wavelet analysis methods, while further analyzing the impacts of EASM/NWPSH on summer precipitation during different periods. The main conclusions are listed as follows:

(1)　The most pronounced periodic variation of precipitation in the Beijing area was observed during the periodicity band of 80–95 years through the entire study period. The less significant period resided over a 32–60 year band spread from 1880 to 2014. Two main periodic oscillations were detected for the EASMI. The most pronounced period at 76–90 year time scales oscillates through the entire study period, with a less significant period at ~45 year time scales from 1880 to 1960. The significant periods oscillate at ~38 year and ~80 year time scales through the entire study period.

(2)　The correlations between summer precipitation in the Beijing area and EASMI/NWPSH at high-frequency were higher compared to those of low-frequency. The most pronounced positive correlation between precipitation and NWPSH was seen in the ~43 year period from 1880 to 1960. Furthermore, the correlation gradually weakened during this periodic scale after 1960. The positive correlation between precipitation and EASM was most significant at a time scale of ~33 years, which sustained from 1960 until the present day. A further heavy precipitation period in the Beijing area was predicted to occur at approximately 2026.

While the current research evaluated the correlation of the EASM and NWPSH with precipitation in the Beijing area, future research efforts should include other oceanic-atmospheric patterns (the PDO and ENSO) and non-climatic factors (urbanization effect and terrain effect). Moreover, a longer study period would be desirable to further investigate changing periodicities.

Author Contributions: Li He and Fuxing Li conceived the study; Fuxing Li processed and wrote the paper; Li He contributed to the revision of the paper.

Conflicts of Interest: The authors declare no conflict of interest.

References

1. Enfield, D.B.; Mestas-Nuñez, A.M.; Trimble, P.J. The Atlantic multidecadal oscillation and its relation to rainfall and river flows in the continental US. *Geophys. Res. Lett.* **2001**, *28*, 2077–2080. [CrossRef]
2. Beebee, R.A.; Michael, M. Variation in the relationship between snowmelt runoff in Oregon and ENSO and PDO. *J. Am. Water Resour. Assoc.* **2004**, *40*, 1011–1024. [CrossRef]
3. Kuss, A.J.M.; Gurdak, J.J. Groundwater level response in US principal aquifers to ENSO, NAO, PDO, and AMO. *J. Hydrol.* **2014**, *519*, 1939–1952. [CrossRef]
4. Anderson, W.P.; Emanuel, R.E. Effect of interannual and interdecadal climate oscillations on groundwater in North Carolina. *Geophys. Res. Lett.* **2008**, *35*. [CrossRef]
5. Peterse, F.; Prins, M.A.; Beets, C.J.; Troelstrab, S.R.; Zheng, H.; Gu, Z.; Schoutena, S.; Damsté, J.S.S. Decoupled warming and monsoon precipitation in East Asia over the last deglaciation. *Earth. Planet. Sci. Lett.* **2011**, *301*, 256–264. [CrossRef]
6. Verdon, D.C.; Wyatt, A.M.; Kiem, A.S.; Franks, S.W. Multidecadal variability of rainfall and streamflow: Eastern Australia. *Water. Resour. Res.* **2004**, *40*. [CrossRef]
7. Kundzewicz, Z.W.; Hirabayashi, Y.; Kanae, S. River floods in the changing climate—Observations and projections. *Water. Resour. Manag.* **2010**, *24*, 2633–2646. [CrossRef]
8. Leng, G.; Tang, Q.; Rayburg, S. Climate change impacts on meteorological, agricultural and hydrological droughts in China. *Glob. Planet. Chang.* **2015**, *126*, 23–34. [CrossRef]
9. Ropelewski, C.F.; Halpert, M.S. Global and regional scale precipitation patterns associated with the El Niño/Southern Oscillation. *Mon. Weather Rev.* **1987**, *115*, 1606–1626. [CrossRef]
10. Hamlet, A.F.; Mote, P.W.; Clark, M.P.; Lettenmaier, D.P. Effects of temperature and precipitation variability on snowpack trends in the Western United States. *J. Clim.* **2005**, *18*, 4545–4561. [CrossRef]
11. Xue, F.; Liu, C.Z. The influence of moderate ENSO on summer rainfall in eastern China and its comparison with strong ENSO. *Chin. Sci. Bull.* **2008**, *53*, 791–800. [CrossRef]
12. Choi, J.; Lu, J.; Son, S.W.; Frierson, D.M.W.; Yoon, J.H. Uncertainty in future projections of the North Pacific subtropical high and its implication for California winter precipitation change. *J. Geophys. Res. Atmos.* **2016**. [CrossRef]
13. Giannini, A.; Saravanan, R.; Chang, P. Oceanic forcing of Sahel rainfall on interannual to interdecadal time scales. *Science* **2003**, *302*, 1027–1030. [CrossRef] [PubMed]
14. Seth, A.; Rauscher, S.A.; Biasutti, M.; Giannini, A.; Camargo, S.J.; Rojas, M. CMIP5 projected changes in the annual cycle of precipitation in monsoon regions. *J. Clim.* **2013**, *26*, 7328–7351. [CrossRef]
15. Diaconescu, E.P.; Gachon, P.; Scinocca, J.; Laprise, R. Evaluation of daily precipitation statistics and monsoon onset/retreat over western Sahel in multiple data sets. *Clim. Dyn.* **2015**, *45*, 1325–1354. [CrossRef]
16. Djebou, S.; Dagbegnon, C.; Singh, V.P. Impact of climate change on precipitation patterns: A comparative approach. *Int. J. Climatol.* **2016**. [CrossRef]
17. Soelen, E.E.; Ohkouchi, N.; Suga, H.; Damsté, J.S.S.; Reichart, G.J. A late Holocene molecular hydrogen isotope record of the East Asian Summer Monsoon in Southwest Japan. *Quat. Res.* **2016**, *86*, 287–294. [CrossRef]
18. Mazon, J.J.; Castro, C.L.; Adams, D.K.; Chang, H.I.; Carrillo, C.M.; Brost, J.J. Objective Climatological Analysis of Extreme Weather Events in Arizona during the North American Monsoon. *J. Appl. Meteorol. Clim.* **2016**, *55*, 2431–2450. [CrossRef]
19. Lahmers, T.M.; Castro, C.L.; Adams, D.K.; Serra, Y.L.; Brost, J.J.; Luong, T. Long-term changes in the climatology of transient inverted troughs over the North American monsoon region and their effects on precipitation. *J. Clim.* **2016**, *29*, 6037–6064. [CrossRef]
20. Djebou, D.C.S. Integrated approach to assessing streamflow and precipitation alterations under environmental change: Application in the Niger River Basin. *J. Hydrol. Reg. Stud.* **2015**, *4*, 571–582. [CrossRef]
21. Jiang, Z.; Yang, S.; He, J.; Li, J.; Liang, J. Interdecadal variations of East Asian summer monsoon northward propagation and influences on summer precipitation over East China. *Meteorol. Atmos. Phys.* **2008**, *100*, 101–119. [CrossRef]
22. Zhou, X.X.; Ding, Y.H.; Wang, P.X. Moisture transport in the Asian summer monsoon region and its relationship with summer precipitation in China. *J. Meteorol. Res.* **2010**, *24*, 31–42.

23. Li, Q.; Wei, F.Y.; Li, D.L. Interdecadal variations of East–Asian summer monsoon and drought/flood distribution over eastern china in last 159 years. *Acta Geogr. Sin.* **2011**, *66*, 25–37. [CrossRef]

24. Liu, J.; Chen, J.; Zhang, X.; Li, Y.; Rao, Z.; Chen, F. Holocene East Asian summer monsoon records in northern China and their inconsistency with Chinese stalagmite δ 18 O records. *Earth Sci. Rev.* **2015**, *148*, 194–208. [CrossRef]

25. Lu, J.M.; Ren, J.Z.; Ju, J.H. The inter-decadal variability of East Asia monsoon and its effect on the rainfall over China. *J. Trop. Meteorol.* **2004**, *10*, 14–22.

26. Ding, Y.; Wang, Z.; Sun, Y. Inter-decadal variation of the summer precipitation in East China and its association with decreasing Asian summer monsoon. Part I: Observed evidences. *Int. J. Climatol.* **2008**, *28*, 1139–1161. [CrossRef]

27. Yu, S.; Shi, X.; Lin, X. Interannual variation of East Asian summer monsoon and its impacts on general circulation and precipitation. *J. Geogr. Sci.* **2009**, *19*, 67–80. [CrossRef]

28. Ding, Y.; Sun, Y.; Wang, Z.; Zhu, Y.; Song, Y. Inter-decadal variation of the summer precipitation in China and its association with decreasing Asian summer monsoon Part II: Possible causes. *Int. J. Climatol.* **2009**, *29*, 1926–1944. [CrossRef]

29. He, X.; Gong, D. Interdecadal change in western Pacific subtropical high and climatic effects. *J. Geogr. Sci.* **2002**, *12*, 202–209.

30. Li, J.; Yu, R.C.; Wang, J.J. Diurnal variations of summer precipitation in Beijing. *Chin. Sci. Bull.* **2008**, *53*, 1933–1936. [CrossRef]

31. Zhang, X.Z.; Ge, Q.S.; Fang, X.Q.; Zheng, J.; Fei, J. Precipitation variations in Beijing during 1860–1897 AD revealed by daily weather records from the Weng Tong–He Diary. *Int. J. Climatol.* **2013**, *33*, 568–576. [CrossRef]

32. Wen, Y.; Xue, L.; Li, Y.; Wei, N.; Lü, A. Interaction between Typhoon Vicente (1208) and the western Pacific subtropical high during the Beijing extreme rainfall of 21 July 2012. *J. Meteorol. Res.* **2015**, *29*, 293–304. [CrossRef]

33. Dolman, A.J. A synoptic overview and moisture trajectory analysis of the "7.21" heavy rainfall event in Beijing. *J. Meteorol. Res.* **2016**, *30*, 103–116.

34. Xing, R.; Ding, Z.; You, S.; Xu, H. Relationship of tropical-cyclone-induced remote precipitation with tropical cyclones and the subtropical high. *Front. Earth Sci.* **2016**, *10*, 595–606. [CrossRef]

35. Zhai, Y.; Guo, Y.; Zhou, J.; Guo, N.; Wang, J.; Teng, Y. The spatio-temporal variability of annual precipitation and its local impact factors during 1724–2010 in Beijing, China. *Hydrol. Process.* **2014**, *28*, 2192–2201. [CrossRef]

36. Li, M.; Xia, J.; Meng, D. Long-term trend analysis of seasonal precipitation for Beijing, China. *J. Resour. Ecol.* **2012**, *3*, 64–72.

37. Li, M.; Xia, J.; Chen, Z.; Meng, D.; Xu, C. Variation analysis of precipitation during past 286 years in Beijing area, China, using non-parametric test and wavelet analysis. *Hydrol. Process.* **2013**, *27*, 2934–2943. [CrossRef]

38. Zhu, J.H.; Wang, S.W. 80a-Oscillation of summer rainfall over the east part of China and East-Asian summer monsoon. *Adv. Atmos. Sci.* **2001**, *18*, 1043–1050.

39. Gao, H.; Jiang, W.; Li, W. Changed relationships between the East Asian summer monsoon circulations and the summer rainfall in eastern China. *J. Meteorol. Res.* **2014**, *28*, 1075–1084. [CrossRef]

40. Li, S.; Yang, S.; Liu, X. The Characteristics of Drought-Flood Variation and Its Influence Factors in Beijing during 1960–2013. *J. Nat. Resour.* **2015**, *30*, 951–962. (In Chinese)

41. Guo, Q. The index of East Asian summer monsoon and its variation analysis. *Acta Geogr. Sin.* **1983**, *38*, 207–217. (In Chinese)

42. Xu, J.J.; Zhu, Q.G.; Shi, N. An analysis of abnormal spectrum in the variation of summer eastern Asian monsoon in the past 100 years. *J. Meteorol.* **1997**, *55*, 620–626.

43. Zhao, F.F.; Xu, Z.X.; Huang, J.X. Monotonic trend and abrupt changes for major climate variables in the headwater catchment of the Yellow River basin. *Hydrol. Process.* **2008**, *22*, 4587–4599. [CrossRef]

44. Zhao, P.; Chen, J.M.; Xiao, D.; Nan, S.L.; Zou, Y.; Zhou, B.T. Summer Asian Pacific oscillation and its relationship with atmospheric circulation and monsoon rainfall. *Acta Meteorol. Sin.* **2008**, *22*, 455–471.

45. Guo, Q.; Cai, J.; Shao, X.; Sha, W. Studies on the variations of East Asian summer monsoon during A D 1873–2000. *Chin. J. Atmos. Sci.* **2004**, *28*, 206–216. (In Chinese)

46. Mu, Q.; Wang, S.; Zhu, J.; Gong, D. Variations of the Western Pacific Subtropical High in Summer during the Last Hundred Years. *Chin. J. Atmos. Sci.* **2001**, *25*, 787–797. (In Chinese)

47. Kumar, P.; Foufoula-Georgiou, E. Wavelet analysis for geo-physical applications. *Rev. Geophys.* **1997**, *35*, 385–412. [CrossRef]

48. Labat, D. Recent advances in wavelet analyses: Part 1. A review of concepts. *J. Hydrol.* **2005**, *314*, 275–288. [CrossRef]

49. Partal, T.; Kucuk, M. Long-term trend analysis using discrete wavelet components of annual precipitations measurements in Marmara region (Turkey). *Phys. Chem. Earth* **2006**, *31*, 1189–1200. [CrossRef]

50. Schaefli, B.; Maraun, D.; Holschneider, M. What drives high flow events in the Swiss Alps? Recent developments in wavelet spectral analysis and their application to hydrology. *Adv. Water Resour.* **2007**, *30*, 2511–2525. [CrossRef]

51. Partal, T. Wavelet analysis and multi-scale characteristics of the runoff and precipitation series of the Aegean region (Turkey). *Int. J. Climatol.* **2012**, *32*, 108–120. [CrossRef]

52. Jevrejeva, S.; Moore, J.C.; Grinsted, A. Influence of the Arctic Oscillation and El Niño-Southern Oscillation (ENSO) on ice conditions in the Baltic Sea: The wavelet approach. *J. Geophys. Res. Atmos.* **2003**, *108*. [CrossRef]

53. Grinsted, A.; Moore, J.C.; Jevrejeva, S. Application of the cross wavelet transform and wavelet coherence to geophysical time series. *Nonlinear Process. Geophys.* **2004**, *11*, 561–566. [CrossRef]

54. Liu, Y.; Brown, J.; Demargne, J.; Seo, D.J. A wavelet-based approach to assessing timing errors in hydrologic predictions. *J. hydrol.* **2011**, *397*, 210–224. [CrossRef]

55. Tremblay, L.; Larocque, M.; Anctil, F.; Rivard, C. Teleconnections and interannual variability in Canadian ground water levels. *J. Hydrol.* **2011**, *410*, 178–188. [CrossRef]

56. Tang, C.; Chen, D.; Crosby, B.T.; Piechotac, T.C.; Wheaton, J.M. Is the PDO or AMO the climate driver of soil moisture in the Salmon River Basin, Idaho? *Glob. Planet. Chang.* **2014**, *120*, 16–23. [CrossRef]

57. Torrence, C.; Webster, P. Interdecadal Changes in the ESNO Monsoon System. *J. Clim.* **1999**, *12*, 2679–2690. [CrossRef]

58. Torrence, C.; Compo, G.P. A practical guide to wavelet analysis. *Bull. Am. Meteorol. Soc.* **1998**, *79*, 61–78. [CrossRef]

59. Wallace, J.M.; Zhang, Y.; Lau, K.H. Structure and seasonality of interannual and interdecadal variability of the geopotential height and temperature-fields in the northern-hemisphere troposphere. *J. Clim.* **1993**, *6*, 2063–2082. [CrossRef]

60. Liang, E.; Eckstein, D.; Liu, H. Climate-growth relationships of relict Pinus tabulaeformis at the northern limit of its natural distribution in northern China. *J. Veg. Sci.* **2008**, *19*, 393–406. [CrossRef]

61. Yim, S.Y.; Wang, B.; Kwon, M.H. Interdecadal change of the controlling mechanisms for East Asian early summer rainfall variation around the mid-1990s. *Clim. Dyn.* **2014**, *42*, 1325–1333. [CrossRef]

62. Hartmann, H.; Becker, S.; King, L. Quasi-periodicities in Chinese precipitation time series. *Theor. Appl. Climatol.* **2008**, *92*, 155–163. [CrossRef]

63. Zhang, Q.; Xu, C.; Jiang, T.; Wu, Y. Possible influence of ENSO on annual maximum streamflow of the Yangtze River, China. *J. Hydrol.* **2007**, *333*, 265–274. [CrossRef]

64. Zhang, Z.; Chao, B.F.; Chen, J.; Wilson, C.R. Terrestrial water storage anomalies of Yangtze River Basin droughts observed by GRACE and connections with ENSO. *Glob. Planet. Chang.* **2015**, *126*, 35–45. [CrossRef]

65. Chen, W.; Kang, L.; Wang, D. The coupling relationship between summer rainfall in China and Global sea surface temperature. *Clim. Environ. Res.* **2006**, *11*, 259–269. (In Chinese)

66. Deng, W.; Sun, Z.; Zeng, G.; Ni, D. Interdecadal variation of summer precipitation pattern over eastern China and its relationship with the North Pacific SST. *Chin. J. Atmos. Sci.* **2009**, *33*, 835–846. (In Chinese)

67. Zhang, C.L.; Chen, F.; Miao, S.G.; Li, Q.C.; Xia, X.A.; Xuan, C.Y. Impacts of urban expansion and future green planting on summer precipitation in the Beijing metropolitan area. *J. Geophys. Res. Atmos.* **2009**, *114*. [CrossRef]

68. Zhong, S.; Qian, Y.; Zhao, C.; Leung, R.; Yang, X.Q. A case study of urbanization impact on summer precipitation in the Greater Beijing Metropolitan Area: Urban heat island versus aerosol effects. *J. Geophys. Res. Atmos.* **2015**, *120*. [CrossRef]